The fabrication and mechanical properties of a novel 3-component auxetic structure for composites

G.H. Zhang*, O. Ghita, K.E. Evans

College of Engineering, Mathematics and Physical Sciences, University of Exeter, North Park Road, Exeter EX4 4QF, UK

*Corresponding author. g.zhang@exeter.ac.uk, guanhuazhang1@gmail.com (G.H.Zhang). Tel: +44 (0) 1392 263617.

Abstract

Functional auxetic composite materials can be fabricated from conventional or from auxetic components. The helical auxetic yarn (HAY) is a very recently invented auxetic reinforcing component for composite materials. This paper investigates the Poisson's ratio behaviour of a further development of the HAY, needed for many practical applications. The 3-component auxetic yarn is based on a stiff wrap fibre (the first component) helically wound around an elastomeric core fibre (the second component) coated by a sheath (the third component). The resultant structure can overcome problems such as slippage of the wrap and changes in wrapping angles previously encountered during the manufacture and utilisation of the two-component HAY. The mechanical performance of conventional and novel systems is investigated; with emphasis on the differences between the engineering and true Poisson's ratio. The importance of the utilisation of a true tensile modulus and a true Poisson's ratio is demonstrated. This is the first time reported in the literature that an experimental auxetic effect analysis of HAYs was carried out by comparing true and engineering Poisson's ratio. We show that depending on the coating thickness of the third component, the 3-component auxetic system can demonstrate auxetic behaviour, and the coating thickness can be employed as a new design parameter to tailor both the Poisson's ratio and modulus of this novel composite reinforcement for a wide range of applications.

Keywords: **A.** Functional composites. **A.** Textile composites. **B.** Mechanical properties. **C.** Deformation. Auxetic

1. Introduction

The Poisson's ratio (v_{xy}) is defined as the negative ratio of the transverse strain (ε_y) to the longitudinal strain (ε_x) in the elastic loading direction. The possibilities of varying this property to improve mechanical performance have been recognised relatively recently [1]. Many of the most interesting benefits are obtained when the Poisson's ratio is negative. Materials with a negative Poisson's ratio are called auxetic materials [2] and exhibit the very unusual property of becoming thicker when stretched and thinner when compressed. Since 1987 a range of auxetic materials have been discovered and fabricated from the macroscopic to the molecular levels. [2-13]. Auxetic materials are of interest due to their counter-intuitive behaviour under deformation mechanisms and enhanced properties as a result of having a negative v [14].

One area attracting increasing attention is the development of auxetic fibres [15-19]. These can be constructed either as single filament, intrinsically auxetic fibres [15-17] or by constructing an auxetic yarn from conventional fibres [20-28]. Auxetic fibres can be woven into technical textiles and utilised for sporting, medical and defence applications [25, 29].

A novel auxetic structure for composites is the helical auxetic yarn (HAY) which comprises of two fibres: an elastomeric core and a stiff wrap fibre in the form of a helically wound structure [21]. When a tensile load is applied the elastomeric core becomes thicker as the stiff wrap straightens out, resulting a lateral expansion of the core fibre, and thereby the HAY exhibiting auxetic behaviour with a large negative Poisson's ratio. This novel auxetic mechanism has been examined in many applications in composites [23, 26] and textiles, such as body armour, sutures, optical sensor [21], blast mitigation, filtration [20], and healthcare [22]. Practical issues that can impair HAY performance include poor conformance between

the core and the wrap fibres and maintaining a consistent wrap angle both during manufacture and in use [23, 25-27]. In addition the yarn may be difficult to handle during textile production because the surface is uneven, resulting in uneven fabrics and slippage of wrap fibre or bunching.

In this paper we propose a novel 3-component auxetic yarn which may offer a solution to these issues. Here we explore the behaviour of a 3-component structure comprising an elastomeric core wrapped by a helix enclosed by a sheath, and demonstrate the properties of this structure at a macroscale, see Fig. 1. It is expected that the sheath should help bind the two components together as well as act as a protective coating. The sheath can also be utilised to tailor the overall properties of the yarn. The aim of this work was to establish whether a 3-component auxetic yarn will overcome previous problems in manufacturing HAY and will whether maintain its auxetic behaviour when a coating is applied.

2. Methods

Silicone rubber gel (VTV750) and catalyst (CAT 740/750) purchased from Renishaw plc was used (10:1 ratio by weight) to prepare the core fibre. The mixed silicone gel was degased for 15 min. Finally, pour the mixed material into a mould frame and allow 24 hour for curing at room temperature. The wrap material used as supplied by Monofil Technik was a twisted ultra high molecular weight polyethylene (UHMWPE) multifilament fibre with high stiffness and strength.

Helical auxetic yarns were carefully manufactured manually to ensure an accurate pre-determined wrap pitch angle (λ) around the helical auxetic yarn. In this work, the initial wrap angle of all helical auxetic yarns was maintained at 40^{o} as it is easier to manufacture in terms of sample scale. Nevertheless, it is well known that the HAY can be manufactured with a

range of wrap angles and a lower initial wrap angle provides a better auxetic performance [24-26]. The 3-component auxetic yarn was fabricated by coating the HAY with a sheath of silicone rubber gel within the same mould frame that has been employed to produce the silicone rubber core fibre. The mould frame was designed and built with three types of channels in diameters 9 mm, 14 mm and 18 mm for manufacturing required core fibres and yarns. The fabricated helical auxetic yarn samples and 3-component auxetic yarn samples are shown in Table 1. Two core fibres in diameters 9 mm and 14 mm were employed to fabricate the helical auxetic yarn and the 3-component auxetic yarn; and three different coating thicknesses in 4 mm, 5 mm and 9 mm were also applied in order to carry out a systematic study. It is expected that the core/wrap diameter ratio and coating thickness will influence the auxetic performance of the structure.

Mechanical testing of all samples in Table 1 were carried out according to ASTM D3822-07 – tensile properties of single textile fibres [30]. Tensile measurements were performed by a Lloyd instruments (www.lloyds-instruments.co.uk) EZ 20 mechanical testing machine using a 500 N load cell at a crosshead speed of 5mm min^{-1}. The sample gauge length was set as 80 mm for all samples and an additional gauge length for optical longitudinal strain measurements was marked onto the sample. Three repeat measurements were performed for each type of sample. A 4.9 MP digital camera (Edmund Optics EO-5012C USB) was used to capture images at regular strain intervals during the tensile test. Acquired images were employed to analyse longitudinal and transverse sample strain. Image analysis and strain measurements for these samples were carried out based on Sloan et al.'s previous work [25].

The cross sectional area of the core, wrap and yarns can be calculated using:

$$A_c = \frac{\pi D_c^2}{4} \quad (1)$$

Instantaneous cross sectional areas and instantaneous longitudinal strains were obtained by acquired images of sample sections. A typical example of sample diameter and longitudinal strain measurements is presented in images (f) and (l) of Fig. 3. The change in cross sectional area of the wrap fibre is neglected for HAYs; the initial cross sectional area of the wrap fibre was employed with instantaneous cross sectional area of the core fibre for computing the instantaneous cross sectional area of HAYs. All the original stress and strain data were smoothed using a polynomial fitting method for removing experimental noise ($R^2 < 0.99$), then the engineering and true tensile modulus were computed from the fittings.

Engineering Poisson's ratio for all samples was calculated using the measured engineering strains ε_y and ε_x.

$$\nu_{xy} = -\frac{\varepsilon_y}{\varepsilon_x} \tag{9}$$

where ν_{xy} is the engineering Poisson's ratio, ε_y is the engineering transverse strain, and ε_x is the engineering longitudinal strain.

However, when a material is not linearly elastic the Poisson's ratio may vary considerably with strain. Hence it is necessary to utilise the instantaneous true strains and determine a strain dependent Poisson's ratio [31]. The instantaneous Poisson's ratio was calculated by taking local tangents from true strain-true strain graphs.

$$\nu_{xy}^{int} = -\frac{\varepsilon_y^{int}}{\varepsilon_x^{int}} \tag{10}$$

where ν_{xy}^{int} is the instantaneous true Poisson's ratio, ε_y^{int} is the instantaneous true transverse strain, and ε_x^{int} is the instantaneous true longitudinal strain.

Small amounts of noise in the dimension data can have a large effect on the Poisson's ratio as well, hence the data should be smoothed to remove unwanted noise in the dimension data [31]. The polynomial fitting method was firstly chosen to smooth the dimension data, and the true Poisson's ratio was computed from the fittings. In some cases, fitting several regressions to separate portions of the data set was carried out to avoid distorting localized effects. In addition, the order of fitting also has an effect on the results and this was also explored.

3. Results and discussion

In this work, eight different samples were tested, starting with the individual fibres used to fabricate the yarn (samples A, B and C), followed by the helical auxetic yarn (samples D and E) and finalising with the novel 3 component intrinsic auxetic yarn (samples F, G and H). If there is no change in cross-sectional area with strain, the engineering stress and engineering tensile modulus can be utilised. However, the true stress and true tensile modulus can be also obtained by determining instantaneous cross-sectional area and instantaneous longitudinal strain. Fig. 2 compares engineering and true stress as well as engineering and true tensile modulus as a function of engineering and true longitudinal strain for one convectional helical auxetic yarn (9 mm silicone core) and one 3-component auxetic yarn (9 mm silicone core and 9mm silicone coating), respectively. Although the true stress and true tensile modulus of the samples were computed from the true instantaneous strain, they were plotted as a function of engineering longitudinal strain for convenient comparison purposes. The Young's modulus of all samples was calculated using the small strain region (0.05-0.25% [32]) of the engineering stress-strain data, as shown in Table 1. The stress-strain and tensile modulus-strain curves for the other samples (E, F and H) are not shown here as they presented similar behaviour in Fig. 2. As the cross-sectional area of the sample is diminishing, the true stress of samples D and G is increasing and becoming larger than their engineering values as shown in Fig. 2a and 2c.

The true tensile modulus of sample D deceased much slower than its engineering tensile modulus, and this was attributed to diminished cross-sectional area of the sample as well. It is interesting to note that both engineering and true tensile modulus of sample G had a sharp increase at a strain of 0.20 due to a strain hardening phenomenon. Overall, the true tensile modulus and engineering tensile modulus of samples D and G differed by approximate 50% at the end of the tensile test, respectively, see Fig. 2b and 2d. Therefore, it is important to use the true tensile modulus in practice as the engineering tensile modulus is not reliable and misleading due to significant strain dependence of component cross-sectional areas [24].

Figure 3 presents images of samples under zero and large longitudinal strains. For pure silicone rubber fibre (Fig. 3a-d), when a tensile load is applied the fibre becomes thinner. Nevertheless, for a helical auxetic yarn and 3--component intrinsic auxetic yarn, when a tensile load is applied the elastomeric core becomes thicker as the wrap straightens out; causing a lateral expansion of the core, see Fig. 3e-n. It is also worth noting that the thickness of coating has a great effect on the auxetic performance as shown in Fig. 3i-n. According to the previous works [24, 25], the auxetic effect of a helical structure can be controlled by selecting specific fibre diameters, components moduli, the initial geometry and also the applied strain. In this work, components moduli and the initial geometry have been maintained and focused on the core/warp diameter ratio, the applied strain as well as a new parameter – coating thickness.

Figure 4 show Poisson's ratio analysis for 9 and 14mm silicone rubber core fibre, respectively (samples A and B). Fig. 4a shows three sets of length and width dimension data. All three samples are getting longer and thinner, and should thus have a positive Poisson's ratio. Fig. 4b shows average width vs length of these three data sets with smoothed dimension

data from polynomial fit in order to filter out unwanted noise so that the true Poisson's ratio can be calculated accurately. The same process has been used to calculate the true Poisson's ratio of 14 mm core. The instantaneous true Poisson's ratio has been plotted as a function of engineering longitudinal strain for convenient comparison purposes. Overall, the true Poisson's ratio of 9 mm and 14 mm core is higher than that of engineering one, as shown in Fig. 4c-d. Both silicone fibres (9 and 14mm) had a typical Poisson's ratio behaviour for an elastomeric material.

Poisson's ratio analysis for the helical auxetic yarn with 9 mm core is shown in Fig. 5 (samples D and E). Fig. 5a shows three data sets of average width vs average length of three data sets. As it described in section 2, for this case it is necessary to consider fitting several regressions to separate portions of the data set to avoid smothering localized effects, as shown in Fig. 5b-d; then smoothed data were used to calculate the instantaneous true Poisson's ratio. Curve fitting was carried out in three regions to calculate the true Poisson's ratio, as shown in Fig 5b-d. For comparison purpose, whole fitting method was also employed to smooth the data, see Fig. 5e and f. Fig. 5g compares the Poisson's ratio for helical auxetic yarn as a function of engineering longitudinal strain with different calculating methods. The silicone core shows a calculated true Poisson's ratio of 0.5 over a strain of 0.4. The engineering Poisson's ratio of the helical auxetic yarn has a positive value at very low strains. This is caused by reduction in warp outer diameter before the core is displacing laterally and becoming helical. At a stain of 0.025 there is a zero-crossing of the Poisson's ratio. After this critical point the engineering Poisson's ratio will become increasingly negative until the wrap straightens out. In comparison to the engineering Poisson's ratio, the true Poisson's ratio of the structure decreases at very low strain and crosses the zero point earlier and starts to have a negative value while the engineering Poisson's ratio remains

positive. This is the onset of true auxetic behaviour of the structure. Both true and engineering Poisson's ratios are negative until the strain reaches 0.25, after this the true Poisson's ratio starts to increase and becomes positive again while the engineering Poisson's ratio remains negative. These phenomena agree very well with previous numerical modelling results of mechanical properties of the HAY [24]. As it was discussed previously, fitting the data set as a whole will blur out localized effects, even at higher order fits (see Fig 5e). Localized effects are diminished and 'real' data is missed with a 4^{th} or 9^{th} order fit at the start and finish of the data set. The true Poisson ratio is a measure of instantaneous behaviour; therefore, it is vital to take into account of every 'real' data point in the calculation. In practice the initial positive Poisson's ratio can be avoided by pre-tensioning, as a consequence, the material will be ready for its appropriate applications.

The ratio of core to wrap diameters is a significant geometric parameter available to tailor the auxetic performance of helical auxetic yarn. Therefore, a helical auxetic yarn with 14 mm silicone rubber core was fabricated (Sample E). Poisson's ratio analysis for this structure was carried out in the same manner as the one with 9 mm core. Fig. 5h compares the engineering and true Poisson's ratio of sample E as well as the core. It indicates that calculated true Poisson's ratio of the core maintains around 0.5, the engineering and true Poisson's ratio become negative at very low strains and at almost same time, then the true Poisson's ratio become positive again while the engineering one remains negative after strain of 0.225. It is interesting to see that the true Poisson's ratio of the helical auxetic yarn approaches that of the core at the end of the data set. Therefore, in practice in order to have Poisson's ratio remains negative the strain definition is essential.

Figure 6 presents Poisson's ratio analysis of 3-component auxetic yarns (samples F, G and H). Fig. 6a shows average width vs average length of three data sets. Similar effect as for HAYs was noticed, the samples were getting longer and thinner at the beginning followed by getting longer and thicker. An apparent decrease in average width of sample F is observed at the end of the demission data. This phenomenon could be due to the internal helical auxetic yarn is becoming thinner and lost contact with its coating material, thereby could not create a lateral expansion of the sample. Separate curve fittings are shown in Fig. 6b-d; it indicates that all curves all well fitted. In comparison to the engineering Poisson's ratio, the true Poisson's ratio of the sample decreases much faster until it becomes negative while the engineering Poisson's ratio approaches zero, see Fig. 6e. A sharp increase at the end of the true Poisson's ratio curve is attributed to the loss of contact between the internal helical auxetic yarn and the coating as the structure of the sample is failed. Fig. 6e demonstrates that a 3-component auxetic yarn will still have an auxetic behaviour after coating process.

A thicker coating was employed to fabricate sample G, which has a 9 mm core and 9 mm coating thickness. In comparison to the pure silicone rubber core fibre, Fig. 6f shows that both engineering and true Poisson's ratio decreases with strain. In Fig. 6f, at strain of around 0.225 the true Poisson's ratio is approaching zero, however, the instantaneous width of the sample is still less than its starting length, and therefore, the true Poisson's ratio remains positive. It demonstrates that the 3-component auxetic yarn with 9 mm core and 9 mm coating is not auxetic.

Sample H was fabricated with a larger 14 mm core and the same wrap using a 4 mm coating thickness. Fig. 6g shows that the engineering Poisson's ratio is decreasing with the strain and approaches zero and becomes negative at the strain of around 0.25. The true Poisson's ratio is

also decreasing with applied strain and crosses zero point much earlier than the engineering Poisson's ratio at the strain of around 0.1, then it becomes increasingly negative until reaches maximum value. A sharp increase to positive at the end of true Poisson's ratio curve is due to a sharp decrease in sample width. Fig. 6g demonstrates that sample H will still have an auxetic behaviour after coating process in terms of its engineering and true Poisson's ratio.

Figure 7 compares the auxetic performance of all samples in terms of their engineering and true Poisson's ratio. Fig. 7a and b shows the effect of changing the core/wrap diameter ratio on the auxetic effect of the sample. Both engineering and true Poisson's ratio demonstrates that the core/wrap diameter ratio has great impact on the auxetic behaviour of the sample and a larger core/wrap diameter ratio provides a better auxetic effect. As the previous work [25] indicated that variation in fibre diameter ratio showed less impact on the auxetic behaviour of a helical auxetic yarn while only the engineering Poisson's ratio was considered and only the wrap fibre was varied to fabricate HAYs. In addition, a larger core/wrap diameter ratio will trigger earlier activation of the auxetic behaviour, as shown in Fig. 7b. This is another design parameter to maximise the negative Poisson's ratio, and thereby the auxetic performance of the sample. As it shows in Fig. 7c-f, both engineering and true Poisson's ratio analysis indicate that the auxetic behaviour of the sample will be diminished after the coating process, and the magnitude of the auxetic effect is decreasing with an increasing of coating thickness, see Fig. 8. Fig. 8 shows the minimum Poisson's ratio of each sample batch vs coating thickness. It also demonstrates that a larger core/wrap diameter ratio will offer a better and earlier auxetic performance of the sample with or without coating.

In order to investigate further the sharp decrease in width noticed at the end of the tensile measurements of the 3-component yarn, a second cycle tensile test was carried out. Fig. 9

presents a comparison of true stress-strain, true tensile modulus and true Poisson's ratio analysis between the first and the second tensile measurements of coated samples. In comparison with the first cycle measurements, it is interesting to note that the true Poisson's ratio analysis of all coated samples from the second cycle tensile measurements are very close to that of pure silicone rubber core. Fig. 9b shows that a sharp decrease of stress value is observed at the end of the first cycle tensile test of sample F, indicating that the sample structure is failed. The true tensile modulus for the first and second cycle tensile tests were computed from the smoothed true stress- true strain data ($R^2 < 0.99$), see Fig. 9c. It indicates that the overall modulus of the second cycle tensile test is much lower than that of the first cycle tensile test. Fig. 10a shows the wrap fibre at the one end of the HAY was disconnected from the core fibre after large strain deformations. The gap between the wrap fibre and the sheath was increased after the second cycle tensile test, see Fig. 10b. Fig. 10c and d show the last images of sample F for the first cycle and the second cycle tensile tests, respectively. They demonstrate that the wrap fibre has not failed as the wrap fibre needs to be completely straight before failure. Therefore, it concluded that the internal helical auxetic yarn was becoming thinner and the interface between the wrap and coating was failed after the first cycle measurement. Thus a large displacement could damage the structure of a 3-component auxetic yarn, as a result of that it would lose its auxetic effect. This is another important design point to be considered in order to maximise the negative Poisson's ratio. In practice the sample length and strain range needs to be carefully controlled in order to ensure the structure is still functionalised in terms of the auxetic effect, and a more compactable coating material will probably offers a solution to the interfacial failure problem. In addition, a high stiffness coating material can possibly improve the stiffness and the strength of composites, but it can also reduce the auxetic effect and the toughness of composites.

4. Conclusions

This work has proposed a novel 3-component auxetic yarn structure and attempted to offer solutions for previous problems in manufacturing HAYs. The 3-component structure proposed here does not only offer a good binding between the core and wrap, but also offers a particularly exciting opportunity to protect potentially fragile high-performance wraps, such as carbon or glass fibre. In addition, applying a sheath with an appropriate coating thickness can avoid uneven fabrics and slippage of wrap fibre. Nevertheless, large strain deformations could cause the two ends of the wrap fibre disconnecting from the core fibre, and resulting the 3-component auxetic structure loses its partial auxetic effect.

This work demonstrates that it is possible to fabricate a 3-component structure with a negative Poisson's ratio. The auxetic behaviour is not diminished by an appropriate layer of coating. However, the magnitude of auxetic effect is decreasing with an increase of coating thickness. When a thick coating is employed, the auxetic effect can be completely eliminated, such as sample G. Therefore, in practice a thin layer of coating is recommended to fabricate a 3-component structure. Note that the coating thickness can be utilised as a new design parameter to tailor the Poisson's ratio of auxetic composite materials for different potential applications.

For highly nonlinear and strain dependent auxetic materials, it is important to be aware of the difference between the true and engineering modulus. The true tensile modulus is always recommended in practice, as the engineering tensile modulus can provide misleading results. In addition, using the engineering Poisson's ratio is not possible to adequately present the instantaneous behaviour of a highly strain dependent material. This is also the case of a 3-component structure which demonstrated a highly strain dependent Poisson's ratio. Several

polynomial fitting methods have been introduced for calculating the true Poisson's ratio. The separate curve fitting method seems to be more appropriate than the whole fitting method.

Acknowledgements

This work is supported by the UK Engineering and Physical Science Research Council (EPSRC grant No. EP/J004553/1). The authors would like also to acknowledge Auxetix Ltd., Wisla Narrow Fabrics Ltd and Fothergill Engineered Fabrics Ltd for industrial support, and to their colleagues Dave Baker and Yat-Tarng Shyng for technical support.

References

1. Greaves, G.N., Greer, A.L., Lakes, R.S., and Rouxel, T., *Poisson's ratio and modern materials.* Nature Materials, 2011. **10**(11): p. 823-837.
2. Evans, K.E., Nkansah, M.A., Hutchinson, I.J., and Rogers, S.C., *Molecular network design.* Nature, 1991. **353**(6340): p. 124-124.
3. Lakes, R., *Foam Structures with a Negative Poisson's Ratio.* Science, 1987. **235**(4792): p. 1038-1040.
4. Caddock, B.D. and Evans, K.E., *Microporous materials with negative Poisson's ratios. I. Microstructure and mechanical properties.* Journal of Physics D: Applied Physics, 1989. **22**(12): p. 1877.
5. Alderson, K.L. and Evans, K.E., *The fabrication of microporous polyethylene having a negative Poisson's ratio.* Polymer, 1992. **33**(20): p. 4435-4438.
6. Baughman, R.H. and Galvao, D.S., *Crystalline networks with unusual predicted mechanical and thermal properties.* Nature, 1993. **365**(6448): p. 735-737.

7. Clarke, J.F., Duckett, R.A., Hine, P.J., Hutchinson, I.J., and Ward, I.M., *Negative Poisson's ratios in angle-ply laminates: theory and experiment.* Composites, 1994. **25**(9): p. 863-868.

8. He, C., Liu, P., and Griffin, A.C., *Toward Negative Poisson Ratio Polymers through Molecular Design.* Macromolecules, 1998. **31**(9): p. 3145-3147.

9. Grima, J.N., Jackson, R., Alderson, A., and Evans, K.E., *Do Zeolites Have Negative Poisson's Ratios?* Advanced Materials, 2000. **12**(24): p. 1912-1918.

10. Brandel, B. and Lakes, R.S., *Negative Poisson's ratio polyethylene foams.* Journal of Materials Science, 2001. **36**(24): p. 5885-5893.

11. Alderson, K.L., Webber, R.S., Kettle, A.P., and Evans, K.E., *Novel fabrication route for auxetic polyethylene. Part 1. Processing and microstructure.* Polymer Engineering & Science, 2005. **45**(4): p. 568-578.

12. Cai, Z., Zhang, Y., Li, J., Xue, F., Shang, Y., He, X., Feng, J., Wu, Z., and Jiang, S., *Real time synchrotron SAXS and WAXS investigations on temperature related deformation and transitions of β-iPP with uniaxial stretching.* Polymer, 2012. **53**(7): p. 1593-1601.

13. Pagliara, S., Franze, K., McClain, C.R., Wylde, G.W., Fisher, C.L., Franklin, R.J.M., Kabla, A.J., Keyser, U.F., and Chalut, K.J., *Auxetic nuclei in embryonic stem cells exiting pluripotency*. Nature Materials, 2014. **13**(6): p. 638-644.

14. Evans, K.E. and Alderson, A., *Auxetic Materials: Functional Materials and Structures from Lateral Thinking!* Advanced Materials, 2000. **12**(9): p. 617-628.

15. Alderson, K.L., Alderson, A., Smart, G., Simkins, V.R., and Davies, P.J., *Auxetic polypropylene fibres:Part 1 - Manufacture and characterisation.* Plastics, Rubber and Composites, 2002. **31**(8): p. 344-349.

16. Ravirala, N., Alderson, A., Alderson, K.L., and Davies, P.J., *Expanding the range of auxetic polymeric products using a novel melt-spinning route.* physica status solidi (b), 2005. **242**(3): p. 653-664.

17. Simkins, V.R., Ravirala, N., Davies, P.J., Alderson, A., and Alderson, K.L., *An experimental study of thermal post-production processing of auxetic polypropylene fibres.* physica status solidi (b), 2008. **245**(3): p. 598-605.

18. Ugbolue, S.C., Kim, Y.K., Warner, S.B., Fan, Q., Yang, C.-L., Kyzymchuk, O., and Feng, Y., *The formation and performance of auxetic textiles. Part I: theoretical and technical considerations.* The Journal of The Textile Institute, 2010. **101**(7): p. 660-667.

19. Alderson, K., Alderson, A., Anand, S., Simkins, V., Nazare, S., and Ravirala, N., *Auxetic warp knit textile structures.* physica status solidi (b), 2012. **249**(7): p. 1322-1329.

20. Hook, P.B., *Uses of Auxetic Fibres*, in *U.S. Patent No. US20070210011 A1*2007.

21. Hook, P.B., Evans, K.E., Hannington, J.P., Hartmann-Thompson, C., and Bunce, T.R., *Composite Materials and Structures, U.S. Patent No. US2007031667*, 2007.

22. Hook, P.B., *Composite fibre and related detection system*, in *U.S Patent No. US20090193906 A1*2009.

23. Miller, W., Hook, P.B., Smith, C.W., Wang, X., and Evans, K.E., *The manufacture and characterisation of a novel, low modulus, negative Poisson's ratio composite.* Composites Science and Technology, 2009. **69**(5): p. 651-655.

24. Wright, J.R., Sloan, M.R., and Evans, K.E., *Tensile properties of helical auxetic structures: A numerical study.* Journal of Applied Physics, 2010. **108**(4).

25. Sloan, M.R., Wright, J.R., and Evans, K.E., *The helical auxetic yarn – A novel structure for composites and textiles; geometry, manufacture and mechanical properties.* Mechanics of Materials, 2011. **43**(9): p. 476-486.

26. Miller, W., Ren, Z., Smith, C.W., and Evans, K.E., *A negative Poisson's ratio carbon fibre composite using a negative Poisson's ratio yarn reinforcement.* Composites Science and Technology, 2012. **72**(7): p. 761-766.

27. Wright, J.R., Burns, M.K., James, E., Sloan, M.R., and Evans, K.E., *On the design and characterisation of low-stiffness auxetic yarns and fabrics.* Textile Research Journal, 2012. **82**(7): p. 645-654.

28. Bhattacharya, S., Zhang, G.H., Ghita, O., and Evans, K.E., *The variation in Poisson's ratio caused by interactions between core and wrap in helical composite auxetic yarns.* Composites Science and Technology, 2014. **102**(0): p. 87-93.

29. Kocer, C., McKenzie, D.R., and Bilek, M.M., *Elastic properties of a material composed of alternating layers of negative and positive Poisson's ratio.* Materials Science and Engineering: A, 2009. **505**(1–2): p. 111-115.

30. ASTM, *D 3822-07. Standard Test Method for Tensile Properties of Single Textile Fibers.* 2007.

31. Smith, C.W., Wootton, R.J., and Evans, K.E., *Interpretation of experimental data for Poisson's ratio of highly nonlinear materials.* Experimental Mechanics, 1999. **39**(4): p. 356-362.

32. ISO, *Plastics -- Determination of tensile properties -- Part 1: General principles,* 2012.

Table 1. Fabricated helical auxetic yarns and 3-component auxetic yarns.

Sample	Type	Silicone core diameter (mm) (+/- 0.1mm)	UHMWPE Wrap diameter (mm) (+/- 0.03mm)	Initial wrap angle (°)	Coating thickness (mm)	Young's modulus (MPa)
A	Fibre	9	-	-	-	2.1 ± 0.3
B	Fibre	14	-	-	-	2.1 ± 0.3
C	UHMWPE wrap	-	0.37	-	-	23,000 ± 3,000
D	Helical auxetic yarn	9	0.37	38.8±1.2	-	2.2 ± 0.9
E	Helical auxetic yarn	14	0.37	39.2± 1.0	-	2.2 ± 0.3
F	3-component intrinsic auxetic yarn	9	0.37	38.3±1.5	5	1.8 ± 0.7
G	3-component intrinsic auxetic yarn	9	0.37	42.1± 1.5	9	2.0 ± 0.3
H	3-component intrinsic auxetic yarn	14	0.37	41.6±1.8	4	1.8 ± 0.2

Figure(s)

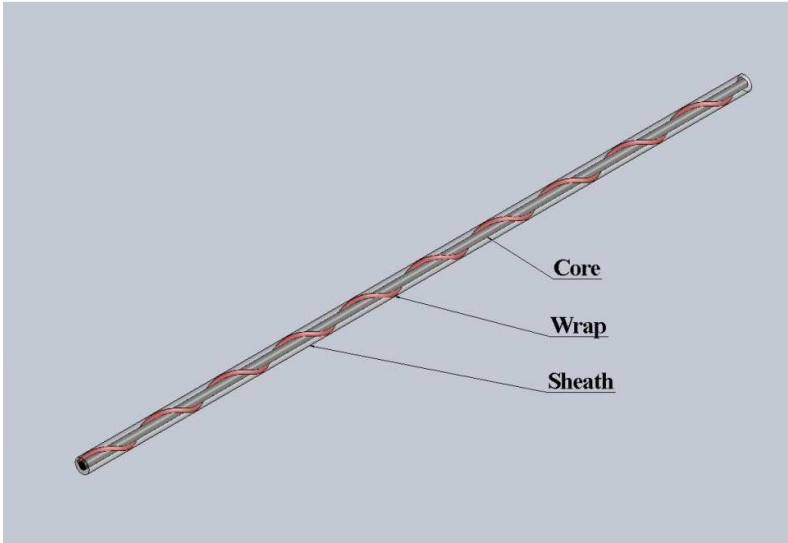

Fig. 1. 3-component auxetic yarn.

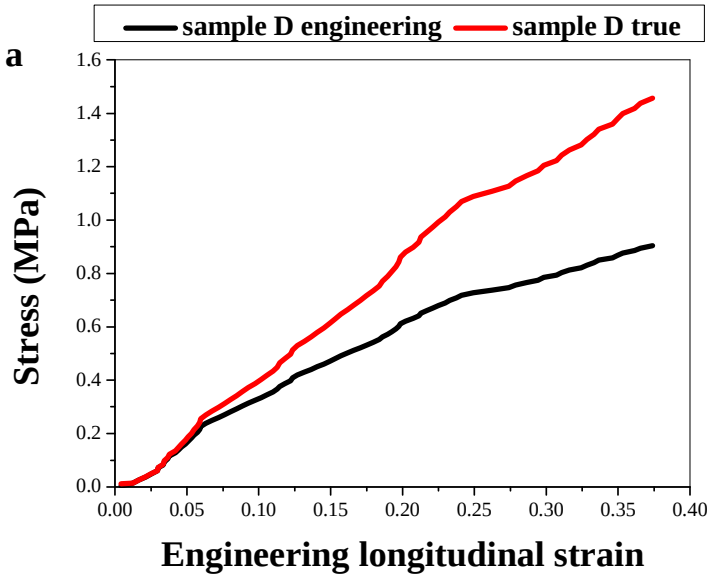

b

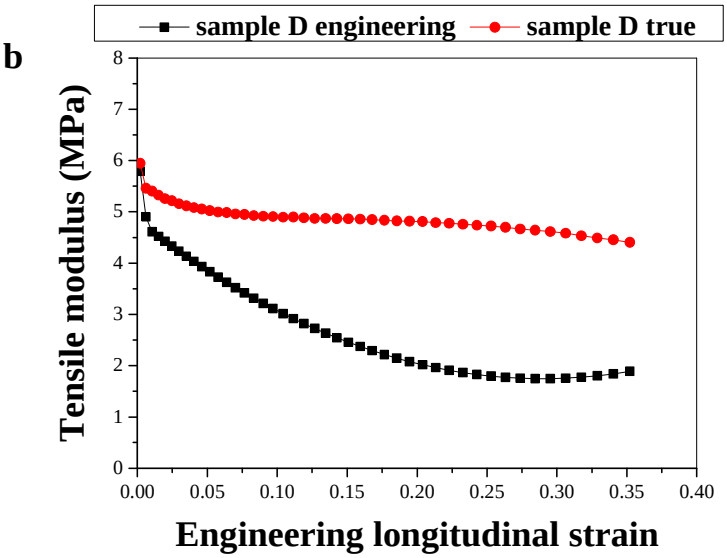
sample D engineering
sample D true
Tensile modulus (MPa)
Engineering longitudinal strain

c

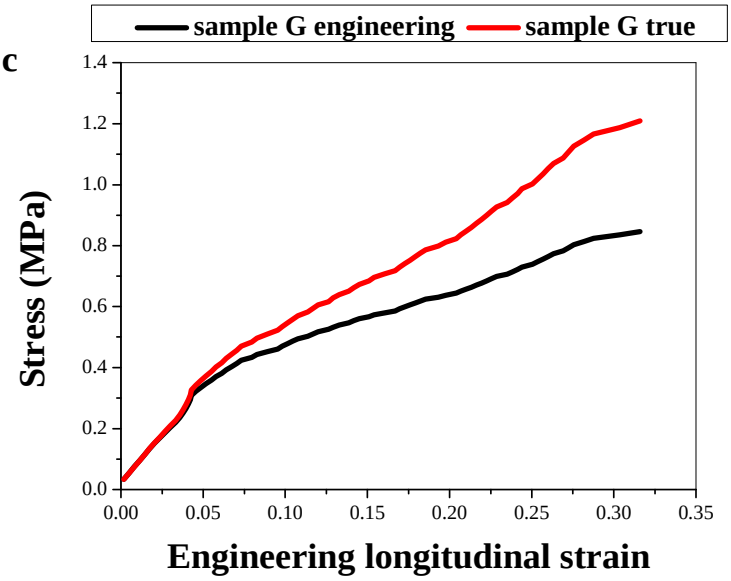
sample G engineering
sample G true
Stress (MPa)
Engineering longitudinal strain

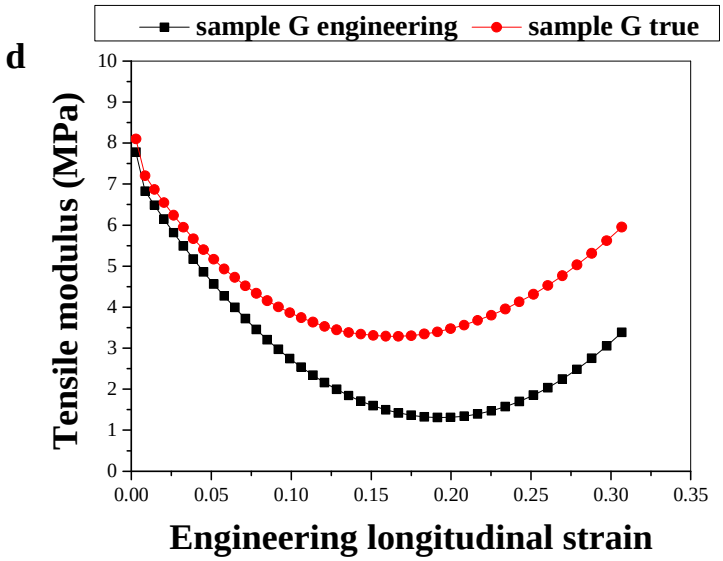

Fig. 2. Tensile modulus analysis for samples D and G: (a) engineering and true stress of sample D; (b) engineering and true tensile modulus of sample D; (c) engineering and true stress of sample G; (d) engineering and true tensile modulus of sample G.

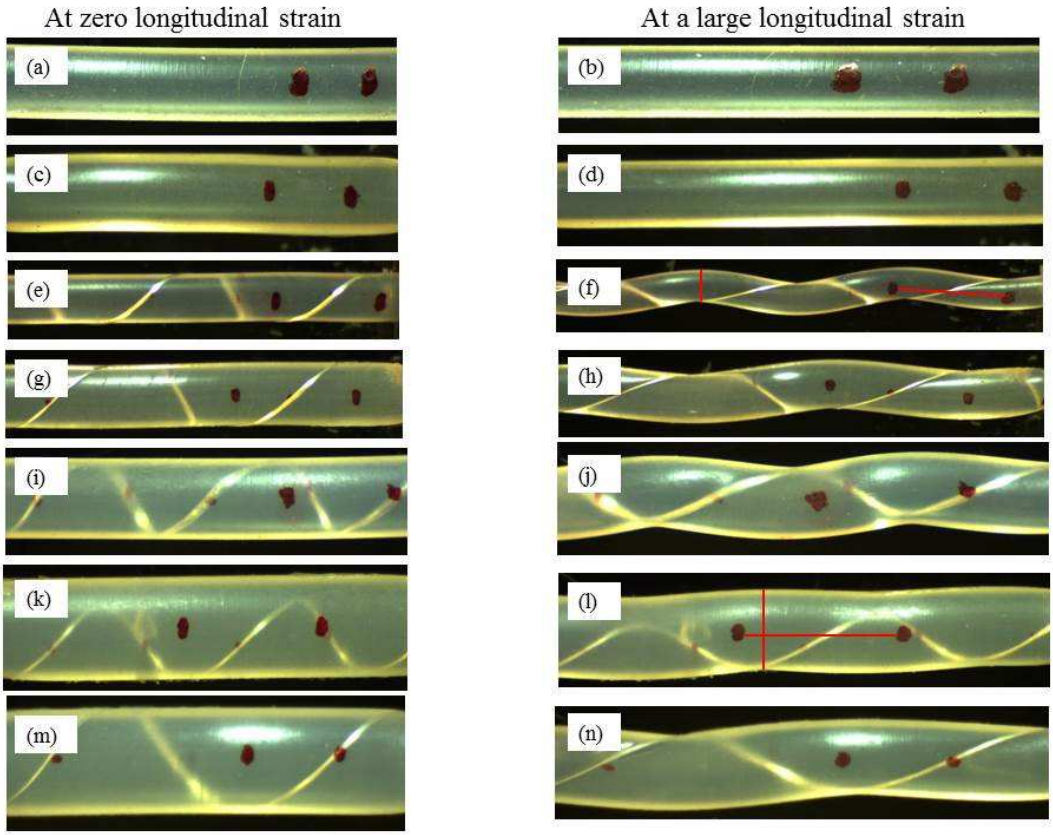

Fig. 3. Deformation measurements for single sample: (a) and (b) 9 mm silicone rubber core(sample A); (c) and (d) 14 mm silicone rubber core (sample B); (e) and (f) helical auxetic yarn with 9 mm core (sample D); (g) and (h) helical auxetic yarn with 14 mm core (sample E); (i) and (j) 3-component auxetic yarn with 9 mm core and 5 mm coating (sample F); (k) and (l) 3-component auxetic yarn with 9 mm core and 9 mm coating (sample G); (m) and (n) 3-component auxetic yarn with 14 mm core and 4 mm coating (sample H) .

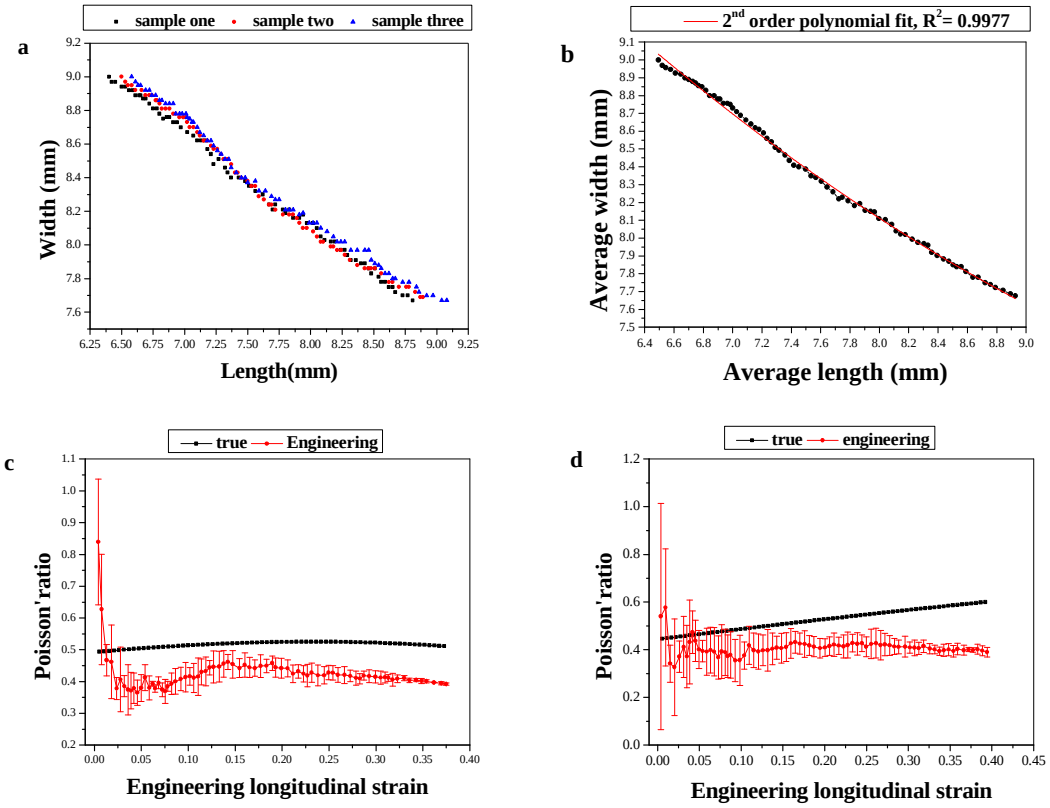

Fig. 4. Poisson's ratio analysis for samples A and B: (a) width vs length of sample A; (b) curve fitting for calculating true Poisson's ratio of sample A; (c) and (d) ν_{xy}^{int} and ν_{xy} vs ε_x of samples A and B.

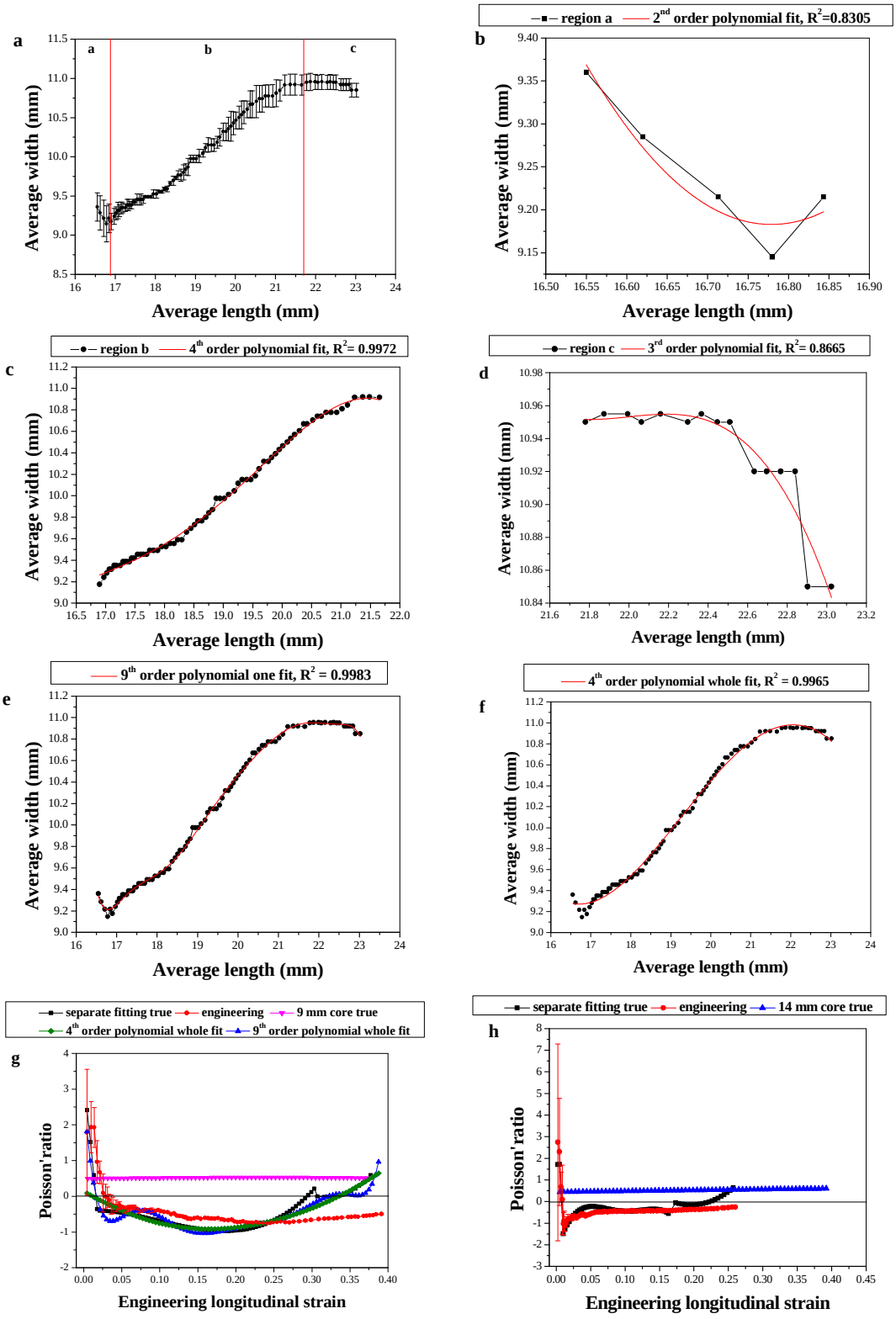

Fig. 5. Poisson's ratio analysis for samples D and E: (a) average width vs average length of sample D; (b) curve fitting for region a of sample D; (c) curve fitting for region b of sample

D; (d) curve fitting for region c of sample D; (e) 9th order one fit of sample D; (f) 4th order one fit of sample D; (g) various ν vs ε_x of sample D; (h) ν_{xy}^{int} and ν_{xy} vs ε_x of sample E.

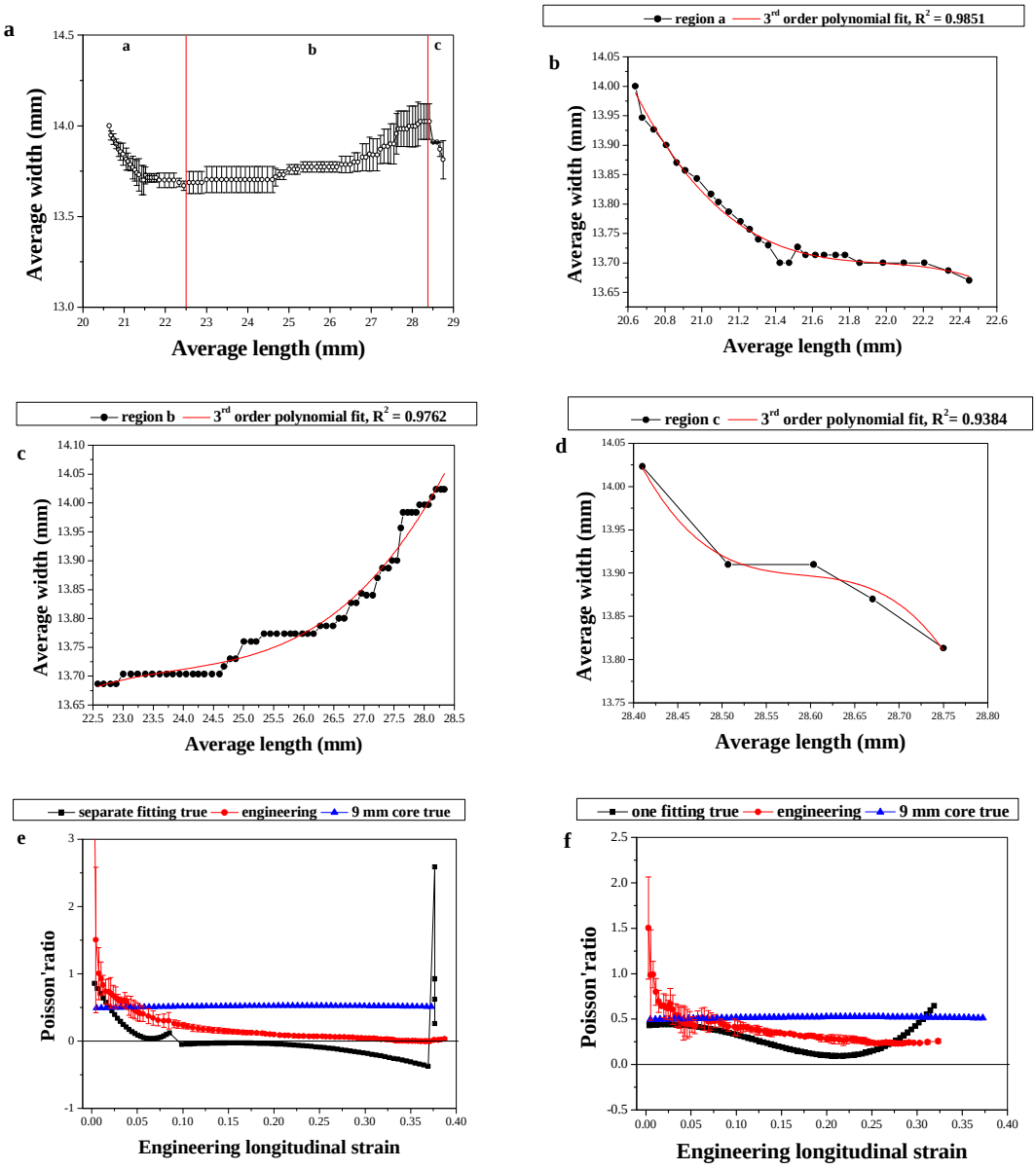

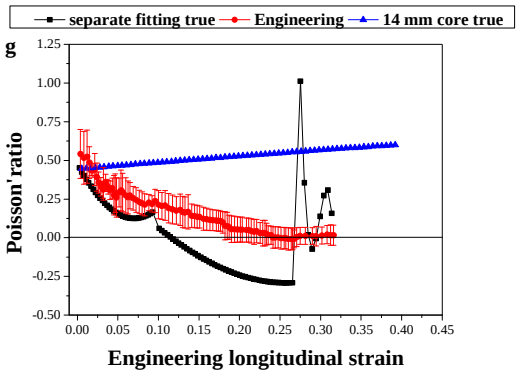

Fig. 6. Poisson's ratio analysis for 3-component auxetic yarns: (a) average width vs average length of sample F; (b) curve fitting for region a of sample F; (c) curve fitting for region b of sample F; (d) curve fitting for region c of sample F; (e) ν_{xy}^{int} and ν_{xy} vs ε_x of sample F. (f) ν_{xy}^{int} and ν_{xy} vs ε_x of sample G; (g) ν_{xy}^{int} and ν_{xy} vs ε_x of sample H.

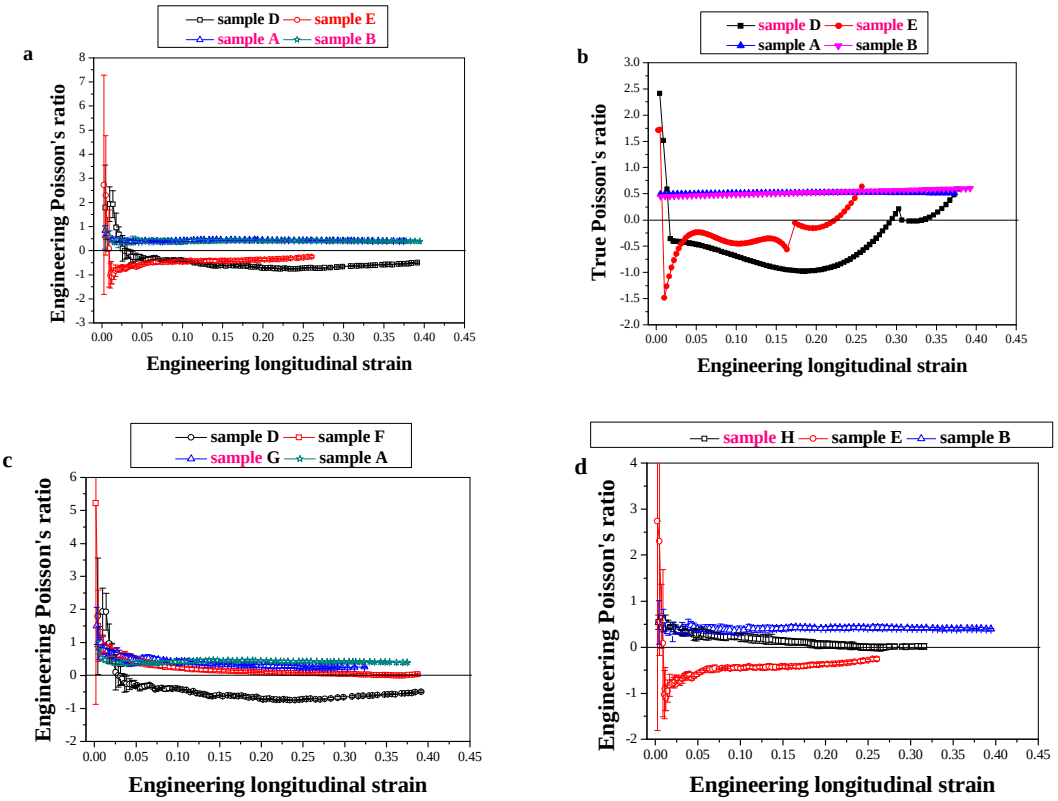

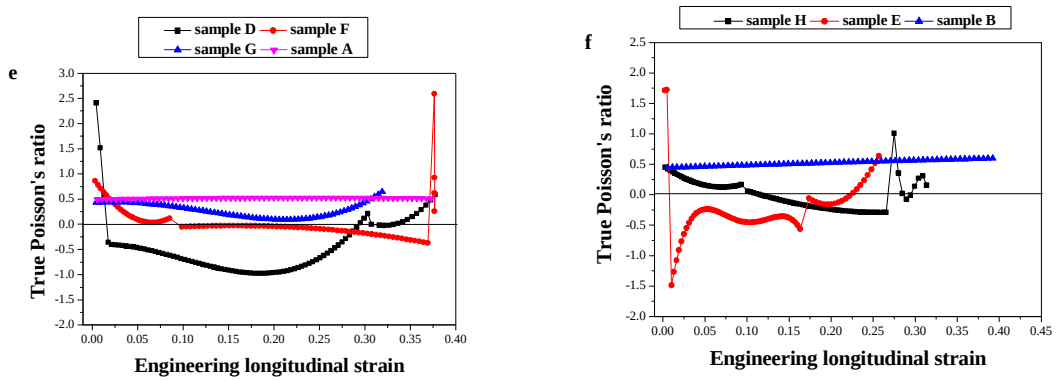

Fig. 7. Comparison of engineering and true Poisson's ratio between samples D, E, F, G and H.

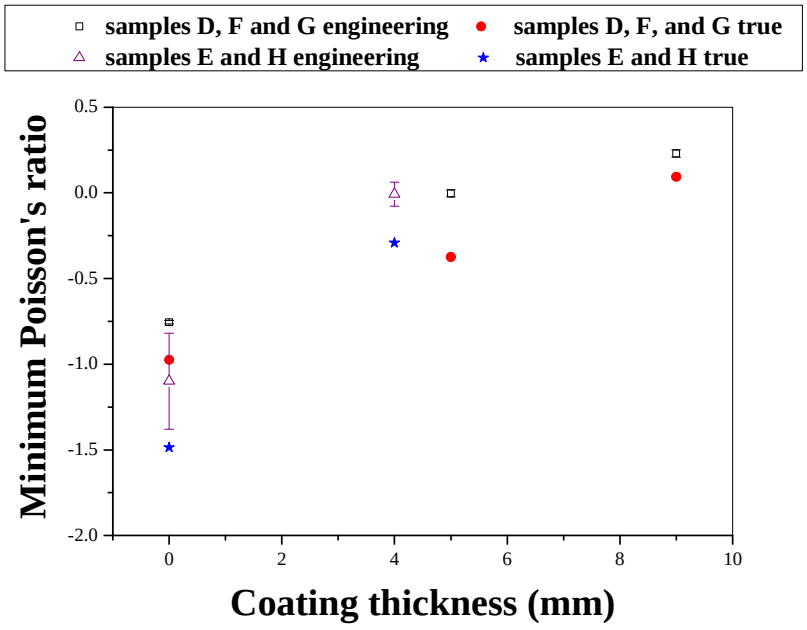

Fig. 8. Minimum Poisson's ratio vs coating thickness of samples D, E, F G, and H.

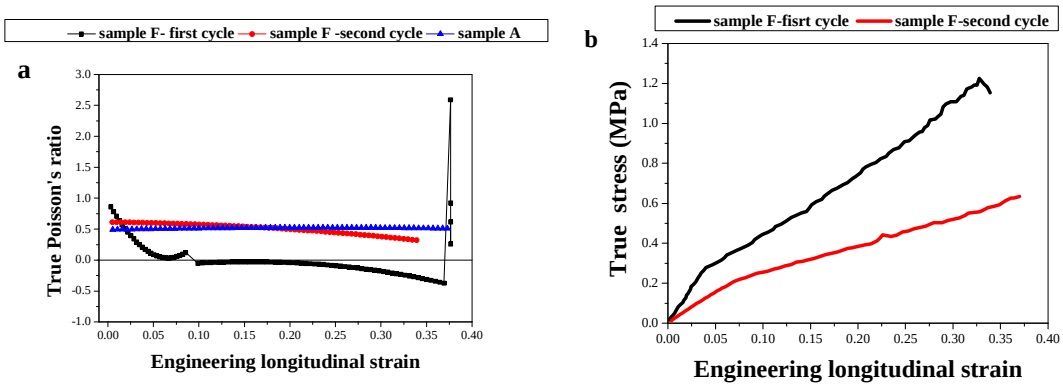

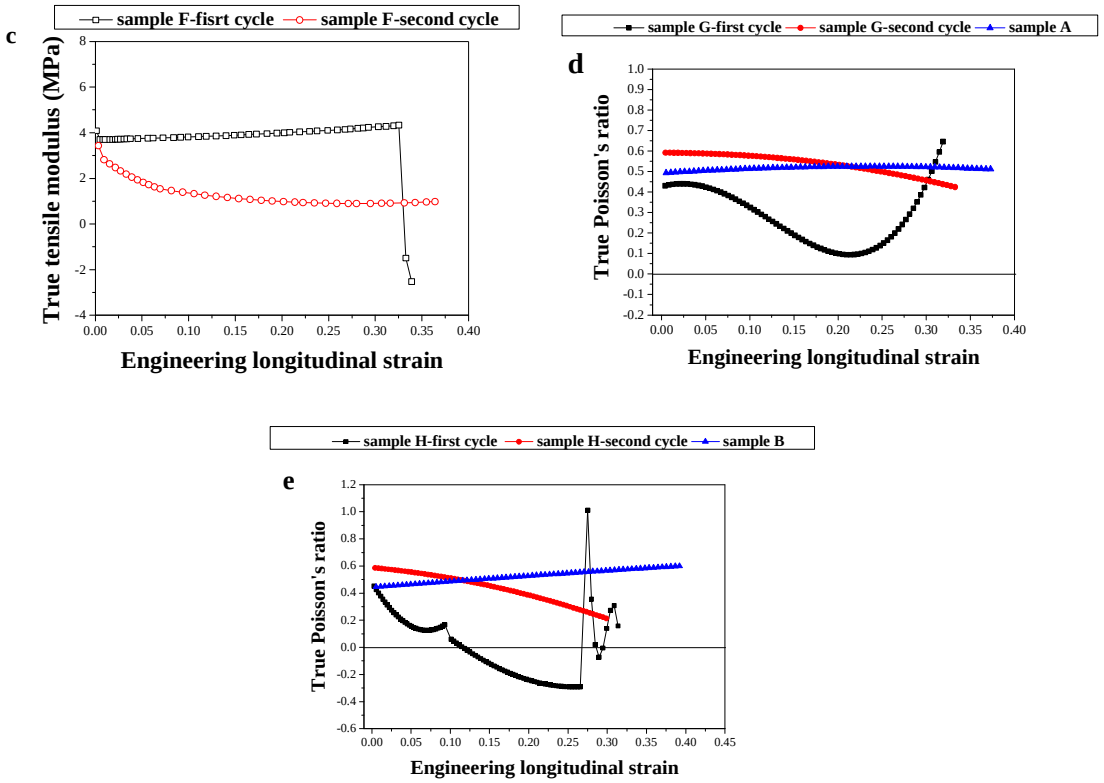

Fig. 9. Comparison of true Poisson's ratio, true stress-strain, and true tensile modulus analysis between the first cycle and second cycle tensile test of samples F(a), (b), (c), G (d) and H (e).

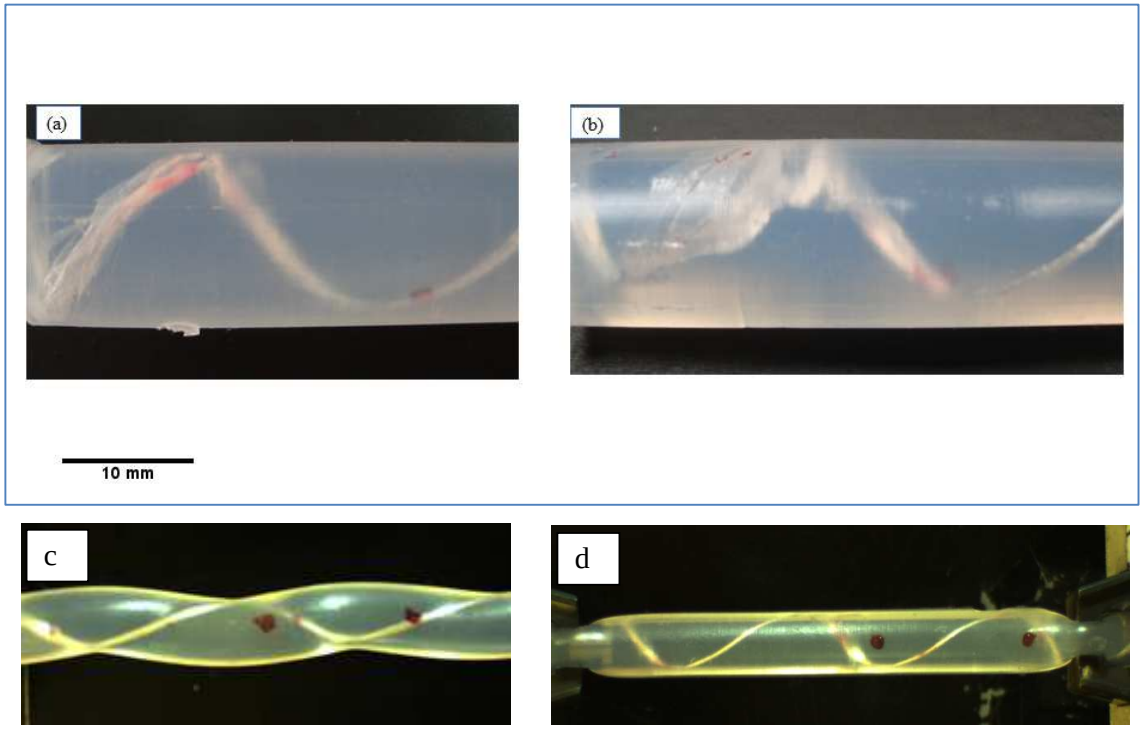

Fig. 10. Pictures of one 3-component auxetic yarn with 9 mm core and 5 mm coating (sample F): (a) interface failure between the wrap fibre and the coating at the one end of the sample after the first cycle tensile test; (b) interface failure between the wrap and the coating at the same end of the sample after the second cycle tensile test; (c) the last image of sample F from the first cycle tensile test; (d) the last image of sample F from the second cycle tensile test.